

# 1 The Palaeo-bathymetry of Base Aptian Salt Deposition 2 on the Northern Angolan Rifted Margin: Constraints 3 from Flexural Backstripping and Reverse Post-breakup 4 Thermal Subsidence Modelling

---

5

6 L. Cowie<sup>1</sup>, R. M. Angelo<sup>1,2</sup>, N. J. Kusznir<sup>1</sup> & G. Manatschal<sup>3</sup>

7 <sup>1</sup>Department of Earth & Ocean Sciences, University of Liverpool, Liverpool, L69 3BX, UK

8 <sup>2</sup>Presently at ConocoPhillips, Houston, TX 77079, USA

9 <sup>3</sup>CNRS-EOST, Université de Strasbourg, 1 rue Blessing, F-67084 Strasbourg, France

## 10 **Abstract**

11 The bathymetric datum with respect to global sea level for Aptian salt deposition in the South  
12 Atlantic is hotly debated. Some models propose that the salt was deposited in an isolated ocean  
13 basin in which local sea level was between 2km and 3km below the global level. In this study, we  
14 use reverse post-breakup subsidence modelling to determine the palaeo-bathymetry of base Aptian  
15 salt deposition on the Angolan rifted continental margin. The reverse post-breakup subsidence  
16 modelling consists of the sequential flexural isostatic backstripping of the post-breakup sedimentary  
17 sequences, decompaction of remaining sedimentary units and reverse modelling of post-breakup  
18 lithosphere thermal subsidence. The reverse modelling of post-breakup lithosphere thermal  
19 subsidence is carried out in 2D and requires knowledge of the continental lithosphere stretching  
20 factor ( $\beta$ ), which is determined from gravity anomaly inversion. The analysis has been applied to the  
21 ION-GXT CS1-2400 deep long-offset seismic reflection profile and the P3 and P7+11 seismic cross  
22 sections of Moulin (2005) and Contrucci et al. (2004) offshore northern Angola. Reverse post-

23 breakup subsidence modelling restores the proximal autochthonous base salt to 200-300m below  
24 global sea level at the time of breakup. In contrast, the predicted water-loaded bathymetries of the  
25 more distal base salt restored to breakup time are much greater, ranging between 1km and 3km.  
26 The predicted bathymetries of the first unequivocal oceanic crust at breakup are approximately  
27 2.5km, as expected for newly formed oceanic crust of 'normal' thickness. Several interpretations of  
28 these results are possible. Our preferred interpretation is that all Aptian salt on the northern Angola  
29 rifted continental margin was deposited 200-300m beneath global sea level and that the proximal  
30 salt subsided by post-rift (post-tectonic) thermal subsidence alone, while the distal salt formed  
31 during late syn-rift when the underlying crust was actively thinning resulting in additional tectonic  
32 subsidence (followed by post-rift thermal subsidence). An alternative interpretation is that the distal  
33 salt is para-autochthonous and moved down-slope into much deeper water during and just after  
34 breakup. We do not believe that a deep isolated ocean basin, with local sea level 2-3km beneath  
35 global sea level as has been proposed, is required to explain the Aptian salt deposition on the  
36 northern Angolan rifted continental margin.

## 37 **Introduction**

38 The northern Angolan rifted continental margin has been the subject of extensive seismic surveys  
39 (Contrucci et al., 2004; Moulin et al., 2005), due to its hydrocarbon resources. The presence of thick  
40 sedimentary packages impacted by a massive middle to upper Aptian salt sequence (up to 5km  
41 thickness in places), makes seismic imaging and interpretation of the sub-salt difficult and presents  
42 major scientific and technical challenges to understanding crustal structure and tectonic history.  
43 Whether the northern Angolan Aptian salt sequence is pre-breakup or post-breakup remains a topic  
44 of major debate; also the palaeo-water depths through the breakup period and the mechanisms  
45 responsible for generating accommodation space through time are uncertain (Jackson et al., 2000;  
46 Karner and Driscoll, 1999; Karner et al., 2003; Karner et al., 1997; Moulin, 2003; Moulin et al., 2005).

47 There is also much debate concerning the geometry and nature of the pre-salt basin, and the  
48 underlying crustal basement structure (Contrucci et al., 2004; Karner and Gambôa, 2007; Nurullina,  
49 2006). Our analysis of the offshore northern Angolan margin is focussed on three profiles in the  
50 Kwanza region; locations are indicated in Figure 1(a). The three profiles include the ION-GXT deep  
51 long offset seismic reflection profile CS1-2400 (Figure 1(c)) and the P3 (Figure 1(d)) and P7+11  
52 profiles (Figure 1(e)) (Contrucci et al., 2004; Moulin et al., 2005). The purpose of this paper is to  
53 provide an understanding of the palaeo-bathymetries of the base Aptian salt deposition (both  
54 proximal and distal) along the northern Angolan rifted continental margin and to understand how  
55 the salt sits within the broad framework of the ocean continent transition (OCT).

## 56 **Reverse post-breakup thermal subsidence modelling**

57 Reconstructed palaeo-bathymetries of base Loeme salt (top Aptian) along the CS1-2400, P3 and  
58 P7+11 profiles has been determined using reverse post-breakup subsidence modelling (Kusznir et al.,  
59 1995; Roberts et al., 1998). The reverse post-breakup subsidence modelling (Figure 2) consists of  
60 the sequential flexural isostatic backstripping of the post-breakup sedimentary sequences,  
61 decompaction of the remaining sedimentary units and reverse modelling of post-breakup  
62 lithosphere thermal subsidence. The magnitude of reverse post-breakup thermal subsidence is  
63 controlled by the continental lithosphere stretching factor ( $\beta$ ) (McKenzie, 1978) which we predict  
64 from gravity anomaly inversion. The magnitude of  $\beta$  therefore controls the restored model elevation  
65 relative to sea level and the predicted palaeo-bathymetry (Roberts et al., 2009; Roberts et al., 1998).  
66 We use the CS1-2400 profile to describe in detail the modelling approach.

67 Continental lithosphere stretching factors ( $\beta$ ) (McKenzie, 1978) range between one and infinity; for  
68 presentation purposes we prefer to use the related parameter, continental lithosphere thinning  
69 factor ( $\gamma = 1 - 1/\beta$ ), which ranges between zero and one.

70 Our gravity anomaly inversion, uses bathymetry (Amante and Eakins, 2009) (Figure 1(a)), satellite  
71 derived free air gravity (Sandwell and Smith, 2009) (Figure 1(b)), sediment thickness data from the  
72 ION-GXT profile (Figure 1(c) and ocean age isochrons (Müller et al., 1997) to determine continental  
73 lithosphere thinning, crustal basement thickness and Moho depth. The gravity anomaly inversion is  
74 carried out in the 3D spectral domain using the scheme of Parker (1972) and also incorporates a  
75 lithosphere thermal gravity anomaly correction to account for the lithosphere mass deficiency from  
76 the elevated geothermal gradient within oceanic and thinned continental margin lithosphere.  
77 Failure to include the lithosphere thermal gravity anomaly correction at rifted continental margins  
78 leads to predictions of Moho depth and crustal basement thickness which are too great and  
79 continental lithosphere thinning factors which are too low. The thermal gravity anomaly correction  
80 is dependent on the thermal re-equilibration time since lithosphere stretching and thinning, and  
81 therefore on continental breakup age. We have used 110Ma as the age of breakup, after Moulin  
82 (2005), for the thermal re-equilibration time to determine the lithosphere thermal gravity anomaly  
83 correction, but have also examined sensitivities to ages for thermal re-equilibration which span the  
84 period Berriasian (140Ma) to early Albian (110Ma). This range corresponds to the start and end of  
85 the main rifting episode in the South Atlantic (Teisserenc and Villemin, 1989). A more detailed  
86 description of the gravity anomaly inversion methodology is described in Chappell and Kusznir  
87 (2008) and Greenhalgh and Kusznir (2007), whilst the example applications are described in Alvey et  
88 al. (2008) and Cowie and Kusznir (2012).

89 Moho depths determined from the gravity anomaly inversion are in good agreement with those  
90 determined from the CS1-2400 seismic reflection profile. Moho depths predicted from gravity  
91 anomaly inversion for sensitivities to reference Moho depth are shown in Figure 3(a). The reference  
92 Moho depth has been calibrated on the CS1-2400 profile using the clear oceanic Moho reflectors.  
93 Calibration (Figure 3(b)) shows that a reference Moho depth of 35.5km is required in order to

94 predict crustal basement thicknesses consistent with those seen in the oceanic domain of the CS1-  
95 2400 seismic reflection profile.

96 A crustal cross section along the CS1-2400 profile (Figure 4(a)) has been constructed using Moho  
97 depths predicted from gravity anomaly inversion assuming the calibrated reference Moho depth of  
98 35.5km; bathymetry and 2D sediment thickness are from the CS1-2400 seismic profile. The  
99 corresponding continental lithosphere thinning factors ( $\gamma$ ) predicted from gravity anomaly inversion,  
100 assuming depth uniform stretching and thinning are shown in Figure 4(b). Continental lithosphere  
101 thinning factors of zero indicate that there has been no stretching or thinning of the continental  
102 lithosphere, whereas a continental lithosphere thinning factor of one indicates that there has been  
103 infinite stretching and thinning of the original continental lithosphere and that no continental crust  
104 or lithosphere remains.

105 Stretching of continental lithosphere leads to a decrease in crustal basement thickness; however,  
106 decompression melting during rifting and seafloor spreading generates oceanic crust, SDRS (seaward  
107 dipping reflectors) and magmatic under plating, which increases crustal basement thickness. A  
108 correction for magmatic addition has been included within the gravity anomaly inversion method,  
109 and uses a parameterization of the decompression melting model of White and McKenzie (1989) to  
110 predict the thickness of the crustal magmatic addition (see Chappell & Kusznir (2008) for a detailed  
111 explanation). Sensitivities to magmatic addition including a normal magmatic and a magma poor  
112 solution have been examined along the CS1-2400 profile (Figure 4(b)). At the western end of the  
113 profile we prefer the normal magmatic solution; however, in the central region of the profile we  
114 believe that the magma poor solution is preferential.

## 115 **Palaeo-bathymetry of the base Aptian salt deposition for the CS1-2400** 116 **profile**

117 Flexural backstripping and decompaction has been applied to the CS1-2400 profile (Figure 5(a) to  
118 remove the salt and post-salt sedimentary layers in order to determine the bathymetry corrected for  
119 sedimentary loading to base salt (Figure 5(b)). Flexural backstripping and decompaction assumes  
120 shaly-sand compaction and density parameters (Sclater and Christie, 1980) during the removal of the  
121 sedimentary layer, whilst the salt layer is given a simple salt lithology (Hudec and Jackson, 2007)  
122 (Table 1).

123 The complex salt movement in this region may appear to be problematic for flexural backstripping.  
124 However, within the palaeo-bathymetric restoration we use the base salt as the target surface for  
125 backstripping, which allows us to ignore the salt movement, as we flexurally backstrip through the  
126 salt to the time of deposition. We are able to disregard the salt movement because as the salt  
127 moved the lithosphere would have responded isostatically to compensate.

128 The bathymetry corrected for sediment loading and decompaction to base salt (Figure 5(b)) is  
129 sensitive to the effective elastic thickness ( $T_e$ ) or lithosphere flexural strength (Bertotti et al., 1998;  
130 Galán and Casallas, 2010; Roberts et al., 1998). The effective elastic thickness depends on the  
131 bending stresses applied to the plate, the rate of stress application, the lithosphere composition and  
132 the geothermal gradient (Kusznir and Karner, 1985). Sensitivities to effective elastic thicknesses of  
133 1.5km, 5km and 10km used in our flexural backstripping have been examined. A finite effective  
134 elastic thickness is required for syn-rift flexural backstripping in order to preserve fault block  
135 topography (Kusznir et al., 1995; Roberts et al., 1998); the use of Airy (local) isostasy in flexural  
136 backstripping (corresponding to  $T_e=0$ km) produces unrealistic internal deformation of individual  
137 fault-blocks. Roberts et al. (1998) showed that effective elastic thicknesses between 1.5km and 5km  
138 are required for syn-rift extensional settings in order to match observed fault block geometries and

139 dips. Roberts et al. (1998) showed that relatively long wavelengths loads of post-rift subsidence and  
140 sediment loading are relatively insensitive to effective elastic thickness. During the post-rift the  
141 lithosphere cools and gets flexurally stronger, therefore, in the post-rift the effective elastic  
142 thicknesses will be larger, which act to freeze in the structures and the short wavelength isostatic  
143 response from the syn-rift. In this study we therefore use a low effective elastic thickness  
144 ( $T_e=1.5\text{km}$ ) appropriate for syn-rift flexurally backstripping.

145 The application of flexural backstripping and decompaction gives an incomplete palaeo-bathymetric  
146 restoration of base salt; we also need to include reverse post-breakup thermal subsidence. We  
147 determine the magnitude of reverse post-breakup thermal subsidence by the continental  
148 lithosphere thinning factor ( $\gamma=1-1/\beta$ ) which we derive from gravity anomaly inversion. Lithosphere  
149 thinning factors from gravity inversion are shown in Figure 5(c); sensitivities for a normal magmatic  
150 solution and a magma poor solution have been examined. At the western end of the CS1-2400  
151 profile the continental lithosphere thinning factors for a normal magmatic solution are 1.0; whereas  
152 for a magma poor solution, the continental lithosphere thinning factors are approximately 0.85. In  
153 the central section of the profile, the continental lithosphere thinning factors, for both solutions  
154 examined, are between 0.7 and 0.85.

155 The restored palaeo-bathymetry to base salt, including reverse thermal subsidence modelling, is  
156 shown in Figure 5(d) assuming a normal magmatic solution and a breakup age of 112Ma. The  
157 proximal base salt restores to just below global sea level with an average bathymetry of  
158 approximately 0.3km. In contrast, the distal base salt does not restore to near sea level; restored  
159 palaeo-bathymetries for the distal base salt (smoothing through fault controlled topography) are  
160 between approximately 0.9km and 2.5km below global sea level. In the deep fault controlled  
161 troughs, palaeo-bathymetries for the distal base salt of approximately 4.0km below sea level are  
162 predicted.

163 Assuming a magma poor solution (Figure 5(e)), the restored palaeo-bathymetry to base salt also  
164 shows that the proximal base salt restores to just below sea level, whilst the distal base salt again  
165 does not. The predicted palaeo-bathymetries of the distal base salt range between approximately  
166 0.9km and 3km below sea level (smoothing through fault controlled topography); in the deep  
167 structural troughs the palaeo-bathymetries are greater (approximately 4.5km below sea level).

168 The lower thinning factors from gravity inversion for the magma poor solution result in less reverse  
169 post breakup thermal subsidence and a slightly greater predicted bathymetry for base salt compared  
170 with the normal magmatic addition solution. The normal magmatic addition solution (Figure 5(d)) is  
171 applicable to the oceanic part of the profile while the magma poor solution (Figure 5(e)) is applicable  
172 to the continental end of the profile, with a transitional region in between.

173 The restoration of base salt palaeo-bathymetry (Figures 5(d) and (e)) using reverse post-breakup  
174 thermal subsidence modelling only restores thermal subsidence. It does not restore syn-rift (syn-  
175 tectonic) subsidence and the consequences of crustal thinning; subsidence arising from syn-tectonic  
176 crust and lithosphere thinning is not included in the restoration.

177 In the oceanic domain, depths of approximately 2.5km ( $\pm$  0.2km depending on magmatic solution),  
178 consistent with an oceanic ridge are predicted, for both a normal magmatic and a magma poor  
179 solution.

180 An additional sensitivity to the continental lithosphere thinning factors, used to drive reverse  
181 thermal subsidence, has been examined for CS1-2400 profile. A continental lithosphere thinning  
182 factor of 1.0 (corresponding to  $\beta=\infty$ ), which gives an upper bound of the restored post-breakup  
183 thermal subsidence, has been applied to the entire profile (Supplementary Figure S1). The predicted  
184 bathymetry for the base of the distal salt remains almost unchanged at between 2km and 3km  
185 below global sea level. This implies that, if the base distal salt was deposited at or just below global  
186 sea level, it has subsided not only due to post-breakup thermal subsidence and sediment loading.



187 Due to the thick sedimentary cover and mobile salt (including salt diapirs and canopies), seismic  
188 imaging of the salt and pre-salt sedimentary units is difficult, which could lead to errors in our  
189 interpretation of the internal structure and thickness of the salt and the pre-salt sedimentary layers.  
190 We are however, more confident in our pick of the base salt. In order to understand the  
191 implications of either over or under estimating the thickness of the salt layer we have examined the  
192 effect of treating the salt layer as a sedimentary layer with a shaly sand lithology within the gravity  
193 inversion and in the reverse post-breakup subsidence modelling (Figure 6). The presence of the salt  
194 layer effects the decompaction and thinning factor estimates. If there was no salt along the margin,  
195 this would result in a deeper Moho (Figure 6(a)) and smaller continental lithosphere thinning factors  
196 (Figure 6(b)) from the gravity inversion, which in turn would lead to less reverse modelled thermal  
197 subsidence and a deeper restoration of the base salt (Figure 6(c)). The largest differences between  
198 the palaeo-bathymetric restorations of the base salt with the salt layer compared to that produced  
199 without the salt layer are seen in the large troughs at the western end of the profile (approximately  
200 0.3km difference). The inclusion or omission of the salt layer does not fundamentally change the  
201 predicted palaeo-bathymetry of base salt.

202 Figure 5 (d and e) are calculated using a breakup age within the gravity inversion and reverse  
203 thermal post-breakup thermal subsidence modelling of 112Ma. Seismic reflection shows a thick pre-  
204 salt sediments up to 8km thick (Unternehrl et al., 2010) beneath the proximal salt which almost  
205 certainly consists of a lower syn-rift sequence with a sag post-rift sequence above. The rift age in this  
206 region is older than breakup and may be as old as 140 Ma (Teisserenc and Villemin, 1989). The  
207 effect of using 140 Ma as the rift age (the age for thermal re-equilibration in the gravity inversion  
208 and reverse thermal subsidence modelling) gives a slightly deeper base proximal salt palaeo-  
209 bathymetry but does not change the overall result that base proximal salt restores to a much  
210 shallower palaeo-bathymetry than the distal salt.

211 In our analysis, we assume depth uniform lithosphere stretching for both the determination of the  
212 lithosphere thermal gravity anomaly correction and the reverse post-breakup thermal subsidence  
213 modelling and thinning. While the possibility of depth dependent lithosphere stretching and thinning  
214 during rifted continental margin formation has been postulated (e.g. Davis and Kusznir (2004)and  
215 Kusznir and Karner (2007)), we prefer to assume depth uniform stretching in the absence of reliable  
216 fault extension observations.

### 217 **Reverse post-breakup subsidence for the P3 and P7+11 profiles**

218 In addition to the CS1-2400 profile, we have also applied the reverse post-breakup thermal  
219 subsidence modelling to the more northerly P3 and P7+11 profiles (Figures 7 and 8). Results are  
220 comparable to those predicted for the CS1-2400 profile; with the proximal base salt restoring to  
221 approximately sea level whilst the distal base salt restores to between 2km and 3km below global  
222 sea level.

223 Predicted thinning factors from gravity inversion, assuming normal magmatic addition, are 1.0 at the  
224 western end of both P3 and P7+P11 profiles consistent with the presence of oceanic crust. Predicted  
225 palaeo-bathymetries for the western end of both profiles are on average 2.85km, consistent with  
226 water depths on newly formed oceanic crust. Continental lithosphere thinning factors predicted  
227 from gravity inversion under the salt are dependent on whether normal or magma poor  
228 decompression melting is assumed. This difference in thinning factor leads to a difference in the  
229 predicted bathymetry of base salt from reverse thermal subsidence modelling. Nonetheless, for both  
230 profiles, the predicted palaeo-bathymetries for base proximal salt are at or just below global sea  
231 level, while the palaeo-bathymetry of base distal salt is between 2km and 3km. At the extreme  
232 eastern end of profile P7+11 the predicted sub aerial exposure of approximately 0.9km is probably  
233 an edge effect from the flexural backstripping or a decompaction artifact.

234 Calibration of the reference Moho depth used within the gravity anomaly inversion, for the P3 and  
235 P7+11 profiles, gives a reference Moho depth of 37.5km, which is larger than that predicted for the  
236 CS1-2400 profile. We have therefore, considered the sensitivity to reference Moho depth within the  
237 reverse post-breakup thermal subsidence modelling (Supplementary Figure S2), using CS1-2400 as  
238 the example. Increasing the reference Moho depth from 35.5km to 37.5km results in a deeper  
239 Moho and smaller continental lithosphere thinning factors predicted from gravity anomaly inversion,  
240 and a deeper restoration of the base salt. The largest differences between the palaeo-bathymetric  
241 restorations of the base salt for a reference Moho depth of 35.5km compared to that produced with  
242 a reference Moho depth of 37.5km are seen in the large troughs at the western end of the profile  
243 (approximately 0.35km difference).

## 244 **Location of the distal salt with respect to COB location along the CS1-** 245 **2400 profile**

246 Knowledge of the horizontal position of the distal salt with respect to the continent-ocean boundary  
247 (COB) and ocean-continent transition (OCT) structure is important for understanding the  
248 depositional context of the base Aptian salt and how the salt sits within the broad framework of the  
249 OCT. The structure of the OCT and COB location have been investigated using gravity anomaly  
250 inversion, sediment corrected residual depth anomaly (RDA) analysis and subsidence analysis. A  
251 detailed description of the methodologies of these techniques is beyond the scope of this paper, but  
252 is described in Cowie (2015).

253 The results from these techniques applied to the CS1-2400 profile are shown in Figure 9. We  
254 interpret the analysis results as showing three distinct crustal zones along the profile: oceanic crust  
255 towards the western end of the profile, hyper-extended continental crust in the centre of the profile,  
256 and continental crust at the eastern end of the profile. The dashed lines indicate the boundary  
257 between each of these interpreted crustal domains; although these interfaces are shown as a sharp

258 line, in reality they are likely to be transitional boundaries. The COB is identified as the ocean ward  
259 start of 'normal' oceanic crust and is identified by changes in crustal basement thickness, inflections  
260 in the RDA analysis signal and also changes in the continental lithosphere thinning from subsidence  
261 analysis and gravity anomaly inversion.

262 In the interpreted oceanic domain at the western end of the profile, crustal basement thicknesses  
263 (Figure 9(a)) predicted from gravity anomaly inversion are approximately 7km, as expected for  
264 oceanic crust. Oceanic crust of normal thickness should have a sediment corrected RDA of  
265 approximately zero, notwithstanding the contribution of mantle dynamic topography. The slightly  
266 positive sediment corrected RDA in this domain (Figure 9(b)) is consistent with the presence of  
267 oceanic crust together with some mantle dynamic uplift, as reported by Crosby & McKenzie (2009)  
268 for the Angolan margin. Continental lithosphere thinning factors from gravity anomaly inversion and  
269 subsidence analysis (Figure 9(c)) are 1.0, also consistent with the presence of oceanic crust. Between  
270 the oceanic domain and the hyper-extended continental crust domain, we see an increase in crustal  
271 basement thickness and the RDA signal, whilst the continental lithosphere thinning factors decrease.  
272 In our interpreted hyper-extended continental crust domain, gravity anomaly inversion predicted  
273 crustal basement thicknesses range between 7km and 12km. The sediment corrected RDA increases  
274 before plateauing at approximately 1000m, whilst the continental lithosphere thinning factors  
275 decrease from 1.0 to between 0.7 and 0.85, which is indicative of thinned continental crust. At the  
276 western end of the hyper-extended continental crust domain, the thinning of the continental crust  
277 may increase together with the start of magmatic addition as ocean crust is approached. Our  
278 interpretation of the presence of hyper-extended continental crust in this domain is significantly  
279 different to that proposed by Unternehr et al. (2010), who proposes the presence of serpentinized  
280 exhumed mantle. Our quantitative analysis results show no evidence of exhumed mantle; exhumed  
281 mantle would show a thinner crust from gravity inversion, lower (negative) sediment corrected RDAs  
282 and higher continental lithosphere thinning factors. At the eastern end of the profile we interpret

283 continental crust as the crustal basement thickness and sediment corrected RDA increases, whilst  
284 the continental lithosphere thinning factors decrease to between 0.2 and 0.4.

285 We have identified the location of the COB on Figure 5, by the dashed line, in order to see where the  
286 salt sits within the OCT. We believe that the majority of the salt along the CS1-2400 profile is  
287 located to the east of the COB and is underlain by hyper-extended continental crust.

## 288 **Discussion**

289 Predicted palaeo-bathymetries have been determined for the base Loeme salt using 2D-flexural  
290 backstripping and decompaction, together with reverse modelling of post-breakup thermal  
291 subsidence. Continental lithosphere thinning factors derived from gravity anomaly inversion have  
292 been used to determine the reverse post-breakup thermal subsidence. Sensitivities to normal  
293 magmatic and magma poor solutions for determining thinning factors from gravity inversion have  
294 been examined. For profile CS1-2400, thinning factors, from both the normal magmatic and magma  
295 poor solutions, used to drive the reverse post-rift thermal subsidence modelling restore the proximal  
296 autochthonous base salt to between 200m and 300m below global sea level at the time of breakup.  
297 A similar palaeo-bathymetry for base proximal salt at breakup is predicted for profile P7-11. For  
298 profile P3, predicted base proximal salt palaeo-bathymetry is slightly shallower with values at or just  
299 below global sea level. In contrast, for all three profiles, reverse post-breakup subsidence modelling  
300 restores the distal base salt to between 2km and 3 km below global sea level. Even if we apply a  
301 continental lithosphere thinning factor of 1.0 to drive the reverse post-rift thermal subsidence along  
302 the full length of the three profiles (which is unreasonable), the palaeo-bathymetries of base distal  
303 salt do not restore to sea level, demonstrating that it is not possible to generate the subsidence of  
304 the base salt by post-rift subsidence alone. The predicted bathymetries at breakup of the first  
305 unequivocal oceanic crust are approximately 2.5km as expected for newly formed oceanic crust of  
306 normal thickness. As previously mentioned, sensitivities to effective elastic thickness and breakup

307 age have been examined. The value of effective elastic thickness does not significantly change the  
308 palaeo-bathymetry predictions. Changing the breakup age has a small effect on the palaeo-  
309 bathymetry predictions but does not change the overall conclusions.

310 We consider several possible explanations of the palaeo-bathymetric restoration of the distal base  
311 salt to water depths substantially below sea level:

312 (i) All the Aptian salt along the northern Angolan profiles was deposited between 200m and 300m  
313 below global sea level, but the distal salt was emplaced during late syn-rift while the continental  
314 crust under it was being actively thinned resulting in additional tectonic subsidence. This is  
315 consistent with seismic evidence, which shows that the distal base salt is extensionally faulted. Also  
316 crustal basement thicknesses from gravity inversion, RDA and subsidence analysis, summarised in  
317 Figure 9, suggest that the distal salt is underlain by hyper-extended continental crust rather than  
318 oceanic crust or exhumed mantle. In contrast to the distal salt, the proximal salt formed in a region  
319 where crustal thinning had already taken place, but had ceased. This interpretation requires that the  
320 distal salt subsides by syn-rift crustal thinning and post-rift thermal subsidence, whilst the proximal  
321 salt subsides by post-rift thermal subsidence alone. Diachronous thinning of the continental crust  
322 from inboard to outboard is to be expected from both observation and modelling, and is consistent  
323 with breakup tectonic models proposed by Péron-Pinvidic and Manatschal (2009), Pindell and  
324 Kennan (2007), Ranero & Perez-Gussinye (2010) and Brune et al. (2014).

325 (ii) An alternative explanation is that during breakup the distal salt moved down-slope to its present  
326 position into much deeper water (and is para-autochthonous). If in the distal regions, the salt is  
327 para-autochthonous (or allochthonous) this suggests that it was not deposited in deep water and  
328 that the salt should not restore to sea level. This interpretation is similar to that advocated in the  
329 Gulf of Mexico by Hudec et al. (2013) and Rowan and Vendeville (2006).

330 (iii) An interpretation which is often invoked (e.g. Burke and Sengör (1988), Burke et al. (2003) and  
331 Karner and Gambôa (2007)) to explain the palaeo-bathymetry of the base Aptian salt along the  
332 northern Angolan margin is that the Aptian salt deposition occurred in confined environmental  
333 conditions (e.g. in a Messinian-type basin, isolated from global sea level). Although a structural  
334 barrier in the south is not dismissed, we believe that there is no definite requirement to invoke an  
335 isolated ocean basin with local sea level 2km and 3km below global sea level for the deposition of  
336 the Aptian salt on the Angolan rifted margin. A strong argument against the isolated basin  
337 interpretation is presented by Pindell et al. (2014) , with reference to the Gulf of Mexico. Pindell et  
338 al. (2014) argue that an isolated basin hypothesis is unlikely as it requires a complicated scenario of  
339 inter-related events to occur. They propose that first rifting must produce a large basin area in  
340 which the depositional surface remains approximately 2km below sea level, there must also be land  
341 barriers, which are able to block out the global sea during the formation of the large basin. Then, at  
342 the time of salt deposition there needs to have been repeated spill/desiccation cycles and a semi-  
343 permeable barrier which continuously allowed just the right amount of sea water into basin so that  
344 shallow-water evaporative conditions were maintained until the end of the salt deposition.

345 Our preferred interpretation of our palaeo-bathymetric restoration of the base Aptian salt along the  
346 northern Angolan profiles is the first interpretation with a possible contribution from the second  
347 interpretation. In summary we believe that both proximal and distal Aptian salt on the Kwanza  
348 margin was deposited at a datum 200-300 m below global sea level, but that the distal salt was  
349 deposited during late syn-rift while the crust under it was being actively thinned which resulted in  
350 additional tectonic subsidence. It is possible that some of the distal salt is para-autochthonous and  
351 moved down-slope to its present day position. It is also possible that syn-tectonic (pre-breakup)  
352 extension continued post-salt deposition in the distal region.

353 **Figure Captions:**

354 **Table 1** – Compaction and density parameters used within the reverse post-breakup thermal  
355 subsidence modelling.

356 [Figure 1](#): Data used in the reverse post-breakup thermal subsidence modelling and gravity anomaly  
357 inversion for the northern Angolan rifted continental margin. (a) Bathymetry (km) (Amante and  
358 Eakins 2009), with the location of profiles CS1-2400, P3 and P7+11 indicated. (b) Satellite derived  
359 free air gravity (mgal) (Sandwell and Smith 2009). (c) Deep long-offset seismic reflection depth  
360 section (PSDM) for the ION-GXT CS1-2400 profile. (d) Seismic velocity model along the P3 profile  
361 (Contrucci et al., 2004; Moulin et al., 2005) from seismic refraction data. (e) Seismic velocity model  
362 along the P7+11 profile (Contrucci et al., 2004; Moulin et al., 2005) from seismic refraction data.

363 [Figure 2](#): Schematic series of sequential cross sections showing reverse post-rift thermal subsidence  
364 modelling from present day to base post-rift for a hypothetical rift basin (Kusznir et al., 1995).

365 [Figure 3](#): Calibration of the reference Moho depth used in the gravity anomaly inversion against  
366 seismic Moho depths for the CS1-2400 profile on the northern Angolan margin. (a) Sensitivity of  
367 Moho depth predicted from gravity anomaly inversion to reference Moho depths of 32.5km, 35km  
368 and 37.5km. (b) Cross-plot of  $\Delta Z_{\text{Moho}}$  (the difference between the gravity inversion predicted  
369 Moho depth and seismic Moho depth) against the value of reference Moho depth used in the gravity  
370 inversion. Calibration gives a reference Moho depth of 35.5km.

371 [Figure 4](#): (a) Crustal cross section along the CS1-2400 profile, showing Moho depth from gravity  
372 anomaly inversion, using the calibrated reference Moho depth of 35.5km. (b) Continental  
373 lithosphere thinning profile, predicted from gravity anomaly inversion, along the CS1-2400 profile.  
374 Sensitivities to a normal magmatic solution and a magma poor solution have been examined. A  
375 normal magmatic solution predicts thinning factors of 1.0 at the western end of the profile and a



376 magma poor solution predicts continental lithosphere thinning factors of approximately 0.85 in this  
377 region.

378 [Figure 5](#): Flexural backstripping and reverse post-breakup thermal subsidence modelling along the  
379 ION-GXT CS1-2400 profile. (a) Digitized present day cross section along the CS1-2400 profile; the  
380 post-salt sedimentary layer is highlighted in blue; pre-salt sedimentary layer in pink; the salt layer is  
381 highlighted in yellow; crust is grey and mantle is red. (b) Sediment corrected bathymetry to base salt  
382 calculated from flexural backstripping and decompaction, using a  $T_e$  of 1.5km. (c) Continental  
383 lithosphere thinning factor profile, from gravity anomaly inversion, for normal magmatic and magma  
384 poor solutions. (d) Reverse post-breakup thermal subsidence modelling along the CS1-2400 profile,  
385 assuming a normal magmatic solution. (e) Reverse post-breakup thermal subsidence modelling  
386 along the CS1-2400 profile, assuming a magma poor solution.

387 [Figure 6](#): Summary of the integrated quantitative analysis results for the CS1-2400 profile used to  
388 determine OCT structure and COB location. (a) Crustal cross section along CS1-2400 profile with  
389 Moho depth from gravity anomaly inversion. (b) The sediment corrected RDA and the RDA  
390 component from variations in crustal basement thickness both have the same general trend along  
391 the profile although the magnitudes differ. This difference gives an indication of the magnitude of  
392 residual topography in this region, which we calculate to be approximately +700m of uplift. (c)  
393 Comparison of continental lithosphere thinning factors determined using subsidence analysis and  
394 gravity anomaly inversion assuming a normal magmatic solution show the same general trend along  
395 profile. The dashed lines on the crustal cross section, RDA and continental lithosphere thinning plots  
396 indicate the distal extent of unequivocal continental crust and its boundary with oceanic crust, which  
397 is a possible interpretation of the COB.

398 [Figure 7](#): Flexural backstripping and reverse post-breakup thermal subsidence modelling along the  
399 P3 profile (Contrucci et al., 2004; Moulin et al., 2005). (a) Digitized present day cross section along

400 the P3 profile; the post-salt sedimentary layers are highlighted in turquoise, orange, green and blue;  
401 pre-salt sedimentary layer in pink; the salt layer is highlighted in yellow; crust is grey and mantle is  
402 red. (b) Sediment corrected bathymetry to base salt calculated from flexural backstripping and  
403 decompaction, using a  $T_e$  of 1.5km. (c) Continental lithosphere thinning factors from gravity  
404 anomaly inversion for a normal magmatic and a magma poor solution. (d) Reverse post-breakup  
405 thermal subsidence modelling along the P3 profile, assuming a normal magmatic solution. (e)  
406 Reverse post-breakup thermal subsidence modelling along the P3 profile, assuming a magma poor  
407 solution.

408 [Figure 8](#): Flexural backstripping and reverse post-breakup thermal subsidence modelling along the  
409 P7+11 profile (Contrucci et al., 2004; Moulin et al., 2005). (a) Digitized present day cross section  
410 along the P3 profile; the post-salt sedimentary layers are highlighted in turquoise, orange, green and  
411 blue; pre-salt sedimentary layer in pink; the salt layer is highlighted in yellow; crust is grey and  
412 mantle is red. (b) Sediment corrected bathymetry to base salt calculated from flexural backstripping  
413 and decompaction using a  $T_e$  of 1.5km. (c) Continental lithosphere thinning factors from gravity  
414 anomaly inversion for a normal magmatic and a magma poor solution. (d) Reverse post-breakup  
415 thermal subsidence modelling along the P7+11 profile, assuming a normal magmatic solution. (e)  
416 Reverse post-breakup thermal subsidence modelling along the P7+11 profile, assuming a magma  
417 poor solution.

418 [Supplementary Figure S1](#): Sensitivity to the effect of over-estimating or under-estimating the  
419 thickness of the salt layer along CS1-2400. Two end member sensitivities have been considered: (i)  
420 having a salt layer (as used in the paper) (labelled “With Salt”) or (ii) treating the salt as just another  
421 sedimentary layer (labelled “No Salt”). (a) Crustal cross section from gravity anomaly inversion,  
422 showing two Moho depths (both using the calibrated reference Moho depth of 35.5km). The Moho  
423 in black is the result of having a salt layer in the gravity anomaly inversion, whereas the Moho in  
424 blue is the result of treating the salt layer as just another sedimentary layer. Removing the salt layer

425 from the gravity anomaly inversion results in a deeper Moho depth prediction. (b) Comparison of  
426 the continental lithosphere thinning factors, predicted from gravity anomaly inversion for the two  
427 sensitivities: with salt (in blue) and no salt (in green). Removing the salt layer from the gravity  
428 anomaly inversion results in smaller continental lithosphere thinning factors. (c) The resulting  
429 palaeo-bathymetries from reverse post-breakup thermal subsidence modelling for the two  
430 sensitivities: with salt (in blue) and no salt (in orange). The “No Salt” sensitivity results in deeper  
431 palaeo-bathymetries, the biggest differences are observed in the central section of the profile.

432 [Supplementary Figure S2](#): Sensitivity to changing the reference Moho depth between 35.5km (as  
433 calibrated for the CS1-2400 profile) to 37.5km (as calibrated for the P3 and P7+11 profiles). (a)  
434 Crustal cross section from gravity anomaly inversion, showing two Moho depths. The Moho in black  
435 is the result of using a reference Moho depth of 35.5km and the Moho in purple is the result of using  
436 a higher reference Moho depth of 37.5km. If we increase the reference Moho depth along the CS1-  
437 2400 profile, this results in a deeper Moho depth prediction. (b) Comparison of the continental  
438 lithosphere thinning factors, predicted from gravity anomaly inversion for the sensitivities to  
439 reference Moho depth. Using a reference Moho depth of 37.5km (in red) results in smaller  
440 continental lithosphere thinning factors along the CS1-2400 profile. (c) The resulting palaeo-  
441 bathymetries from reverse post-breakup thermal subsidence modelling for the two sensitivities to  
442 reference Moho depth: using a reference Moho depth of 35.5km (in blue) and using a reference  
443 Moho depth of 37.5km (in green). The larger reference Moho depth of 37.5km results in deeper  
444 palaeo-bathymetries; the biggest differences are observed in the central section of the profile.

445

446 **References:**

- 447 Alvey, A., Gaina, C., Kuszniir, N. J., and Torsvik, T. H., 2008, Integrated crustal thickness mapping and  
448 plate reconstructions for the high Arctic: *Earth and Planetary Science Letters*, v. 274, no. 3-4,  
449 p. 310-321.
- 450 Amante, C., and Eakins, B. W., 2009, ETOPO1 1 Arc-Minute Global Relief Model: Procedures, Data  
451 Sources and Analysis: NOAA Technical Memorandum NESDIS NGDC-24, p. 19.
- 452 Bertotti, G., Picotti, V., and Cloetingh, S., 1998, Lithospheric weakening during “retroforeland” basin  
453 formation: Tectonic evolution of the central South Alpine foredeep: *Tectonics*, v. 17, no. 1, p.  
454 131-142.
- 455 Burke, K., MacGregor, D. S., and Cameron, N. R., 2003, Africa’s petroleum systems: four tectonic  
456 ‘Aces’ in the past 600 million years: Geological Society, London, Special Publications, v. 207,  
457 no. 1, p. 21-60.
- 458 Burke, K., and Sengör, A. M. C., 1988, Ten metre global sea-level change associated with South  
459 Atlantic Aptian salt deposition: *Marine Geology*, v. 83, no. 1–4, p. 309-312.
- 460 Chappell, A. R., and Kuszniir, N. J., 2008, Three-dimensional gravity inversion for Moho depth at rifted  
461 continental margins incorporating a lithosphere thermal gravity anomaly correction:  
462 *Geophysical Journal International*, v. 174, no. 1, p. 1-13.
- 463 Contrucci, I., Matias, L., Moulin, M., Géli, L., Klingelhofer, F., Nouzé, H., Aslanian, D., Olivet, J.-L.,  
464 Réhault, J.-P., and Sibuet, J.-C., 2004, Deep structure of the West African continental margin  
465 (Congo, Zaïre, Angola), between 5°S and 8°S, from reflection/refraction seismics and gravity  
466 data: *Geophysical Journal International*, v. 158, no. 2, p. 529-553.
- 467 Cowie, L., 2015, Determination of Ocean Continent Transition Structure, Continent Ocean Boundary  
468 Location and Magmatic Type at Rifted Continental Margins [PhD: University of Lierpool, 280  
469 p.
- 470 Cowie, L., and Kuszniir, N., 2012, Mapping crustal thickness and oceanic lithosphere distribution in  
471 the Eastern Mediterranean using gravity inversion: *Petroleum Geoscience*, v. 18, no. 4, p.  
472 373-380.
- 473 Crosby, A. G., and McKenzie, D., 2009, An analysis of young ocean depth, gravity and global residual  
474 topography: *Geophysical Journal International*, v. 178, no. 3, p. 1198-1219.
- 475 Davis, M., and Kuszniir, N., 2004, Depth Dependant lithospheric Stretching at Rifted Continental  
476 Margins, *in* Karner, G. D., Taylor, B., Driscoll, N. W., and Kohlstedt, D. L., eds., *Rheology and  
477 Deformation of the Lithosphere at Continental Margins*, Columbia University Press, p. 408.
- 478 Galán, R. A., and Casallas, I. F., 2010, DETERMINATION OF EFFECTIVE ELASTIC THICKNESS OF THE  
479 COLOMBIAN ANDES USING SATELLITE-DERIVED GRAVITY DATA: *Earth Sciences Research  
480 Journal*, v. 14, p. 7-16.
- 481 Greenhalgh, E. E., and Kuszniir, N. J., 2007, Evidence for thin oceanic crust on the extinct Aegir Ridge,  
482 Norwegian Basin, NE Atlantic derived from satellite gravity inversion: *Geophysical Research  
483 Letters*, v. 34, no. 6, p. L06305.
- 484 Hudec, M. R., and Jackson, M. P. A., 2007, Terra infirma: Understanding salt tectonics: *Earth-Science  
485 Reviews*, v. 82, no. 1–2, p. 1-28.
- 486 Hudec, M. R., Norton, I. O., Jackson, M. P. A., and Peel, F. J., 2013, Jurassic Evolution of the Gulf of  
487 Mexico Salt Basin: *AAPG Bulletin*, v. 97, no. 1, p. 1683 - 1710.
- 488 Jackson, M. P. A., Cramez, C., and Fonck, J.-M., 2000, Role of subaerial volcanic rocks and mantle  
489 plumes in creation of South Atlantic margins: implications for salt tectonics and source  
490 rocks: *Marine and Petroleum Geology*, v. 17, no. 4, p. 477-498.
- 491 Karner, G. D., and Driscoll, N. W., 1999, Tectonic and stratigraphic development of the West African  
492 and eastern Brazilian Margins: insights from quantitative basin modelling: Geological  
493 Society, London, Special Publications, v. 153, no. 1, p. 11-40.

494 Karner, G. D., Driscoll, N. W., and Barker, D. H. N., 2003, Syn-rift regional subsidence across the West  
495 African continental margin: the role of lower plate ductile extension: Geological Society,  
496 London, Special Publications, v. 207, no. 1, p. 105-129.

497 Karner, G. D., Driscoll, N. W., McGinnis, J. P., Brumbaugh, W. D., and Cameron, N. R., 1997, Tectonic  
498 significance of syn-rift sediment packages across the Gabon-Cabinda continental margin:  
499 Marine and Petroleum Geology, v. 14, no. (7-8), p. 973-1000.

500 Karner, G. D., and Gambôa, L. A. P., 2007, Timing and origin of the South Atlantic pre-salt sag basins  
501 and their capping evaporites: Geological Society, London, Special Publications, v. 285, no. 1,  
502 p. 15-35.

503 Kuszniir, N., and Karner, G., 1985, Dependence of the flexural rigidity of the continental lithosphere  
504 on rheology and temperature: Nature, v. 316, no. 6024, p. 138-142.

505 Kuszniir, N. J., and Karner, G. D., 2007, Continental lithospheric thinning and breakup in response to  
506 upwelling divergent mantle flow: application to the Woodlark, Newfoundland and Iberia  
507 margins: Geological Society, London, Special Publications, v. 282, no. 1, p. 389-419.

508 Kuszniir, N. J., Roberts, A. M., and Morley, C. K., 1995, Forward and reverse modelling of rift basin  
509 formation: Geological Society, London, Special Publications, v. 80, no. 1, p. 33-56.

510 McKenzie, D., 1978, Some Remarks on the Development of Sedimentary Basins Earth and Planetary  
511 Science Letters, v. 40, p. 25-32.

512 Moulin, M., 2003, Etude géologique et géophysique des marges continentales passives: exemple du  
513 Zaïre et de l'Angola [PhD: University de Bretagne Occidentale, 360 p.

514 Moulin, M., Aslanian, D., Olivet, J.-L., Contrucci, I., Matias, L., Géli, L., Klingelhofer, F., Nouzé, H.,  
515 Réhault, J.-P., and Unternehr, P., 2005, Geological constraints on the evolution of the  
516 Angolan margin based on reflection and refraction seismic data (ZaiAngo project):  
517 Geophysical Journal International, v. 162, no. 3, p. 793-810.

518 Müller, R. D., Roest, W. R., Royer, J.-Y., Gahagan, L. M., and Sclater, J. G., 1997, Digital isochrons of  
519 the world's ocean floor: Journal of Geophysical Research, v. 102, no. B2, p. 3211-3214.

520 Nurullina, R., 2006, Angola margin : regional tectonic evolution based on integrated analysis of  
521 seismic reflection and potential field data and modelling [Master: University of Oslo.

522 Parker, R. L., 1972, The Rapid Calculation of Potential Anomalies: Geophysical Journal of the Royal  
523 Astronomical Society, v. 31, no. 4, p. 447-455.

524 Péron-Pinvidic, G., and Manatschal, G., 2009, The final rifting evolution at deep magma-poor passive  
525 margins from Iberia-Newfoundland: a new point of view: International Journal of Earth  
526 Sciences, v. 98, no. 7, p. 1581-1597.

527 Pindell, J., Graham, R., and Horn, B., 2014, Rapid outer marginal collapse at the rift to drift transition  
528 of passive margin evolution, with a Gulf of Mexico case study: Basin Research, p. n/a-n/a.

529 Pindell, J. L., and Kennan, L., 2007, Rift models and the salt-cored marginal wedge in the northern  
530 Gulf of Mexico: implications for deep water paleogene Wilcox deposition and basinwide  
531 maturation: Transactions of GCSSEPM 27th Annual Bob F. Perkins Research Conference, p.  
532 146-186.

533 Roberts, A. M., Corfield, R. I., Kuszniir, N. J., Matthews, S. J., Hansen, E.-K., and Hooper, R. J., 2009,  
534 Mapping palaeostructure and palaeobathymetry along the Norwegian Atlantic continental  
535 margin: Møre and Vøring basins: Petroleum Geoscience, v. 15, no. 1, p. 27-43.

536 Roberts, A. M., Kuszniir, N. J., Yielding, G., and Styles, P., 1998, 2D flexural backstripping of  
537 extensional basins; the need for a sideways glance: Petroleum Geoscience, v. 4, no. 4, p.  
538 327-338.

539 Rowan, M. G., and Vendeville, B. C., 2006, Foldbelts with early salt withdrawal and diapirism:  
540 Physical model and examples from the northern Gulf of Mexico and the Flinders Ranges,  
541 Australia: Marine and Petroleum Geology, v. 23, no. 9-10, p. 871-891.

542 Sandwell, D. T., and Smith, W. H. F., 2009, Global marine gravity from retracked Geosat and ERS-1  
543 altimetry: Ridge segmentation versus spreading rate: J. Geophys. Res., v. B01411, no.  
544 114(B1).

545 Sclater, J. G., and Christie, P. A. F., 1980, Continental stretching: An explanation of the Post-Mid-  
546 Cretaceous subsidence of the central North Sea Basin: *Journal of Geophysical Research: Solid*  
547 *Earth*, v. 85, no. B7, p. 3711-3739.

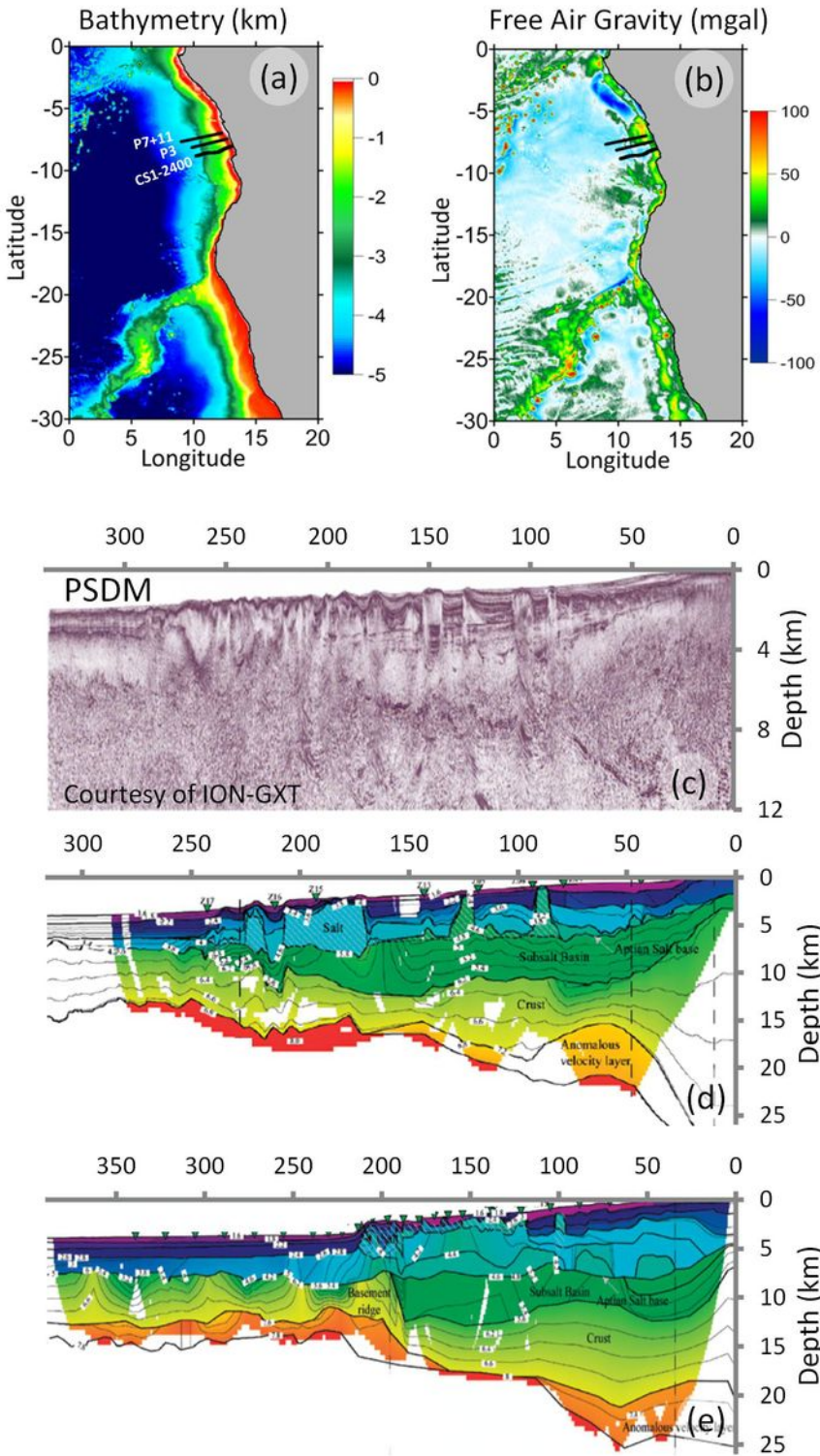
548 Teisserenc, P., and Villemin, J., 1989, Sedimentary basin of Gabon – geology and oil systems, *in*  
549 Edwards, J. D., and Santogrossi, P. A., eds., *Divergent / Passive Margin Basins*. Memoir of the  
550 American Association of Petroleum Geologists, Volume 48.

551 Unternehr, P., Péron-Pinvidic, G., Manatschal, G., and Sutra, E., 2010, Hyper-extended crust in the  
552 South Atlantic: in search of a model: *Petroleum Geoscience*, v. 16, no. 3, p. 207-215.

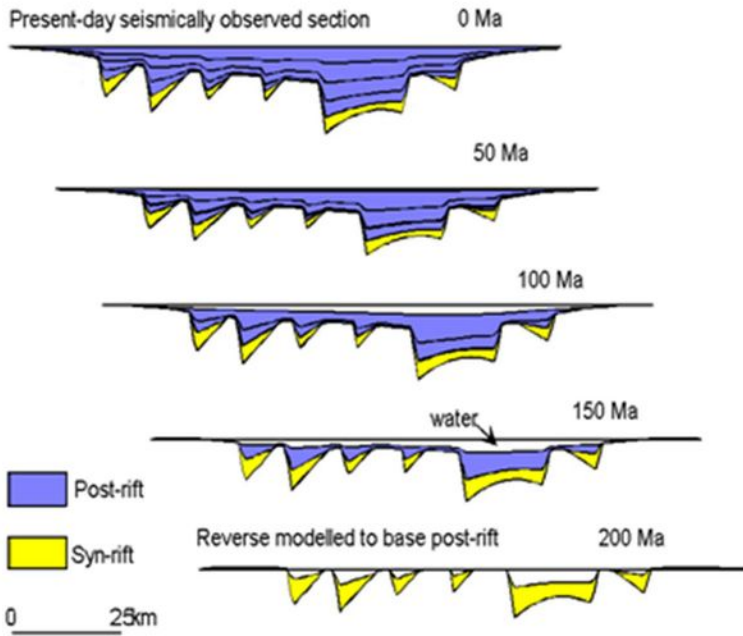
553 White, R., and McKenzie, D., 1989, Magmatism at Rift Zones: The Generation of Volcanic Continental  
554 Margins and Flood Basalts: *Journal of Geophysical Research*, v. 94, no. B6, p. 7685-7729.

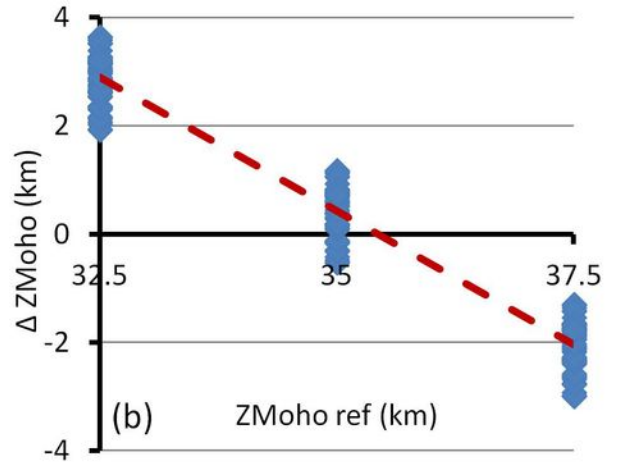
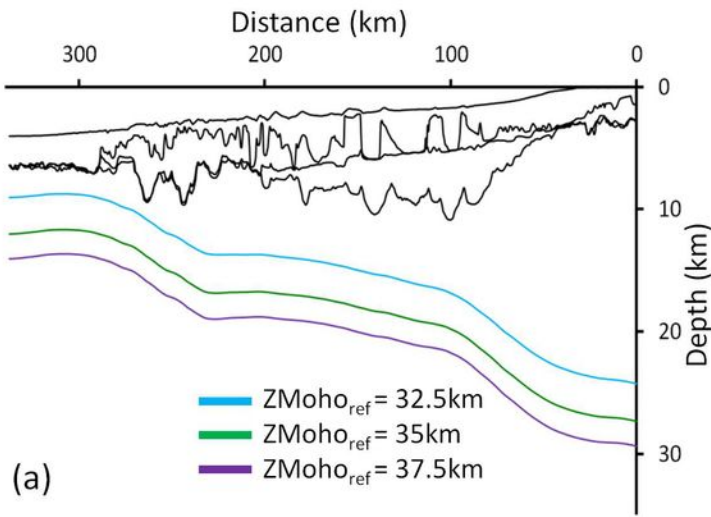
555  
556

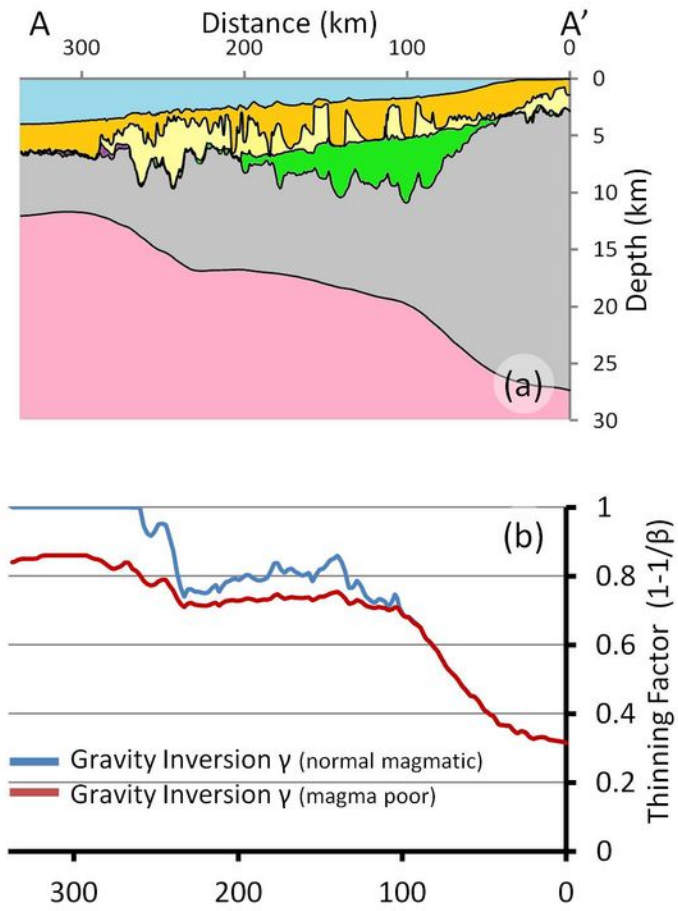
Layer	Lithology	Porosity	Compaction Coefficient (km <sup>-1</sup> )	Density (kgm <sup>-3</sup> )
Post Salt	Shaly-Sand	63	0.51	2720
Salt	Salt	0	0	2200
Pre-salt	Shaly-Sand	63	0.51	2720



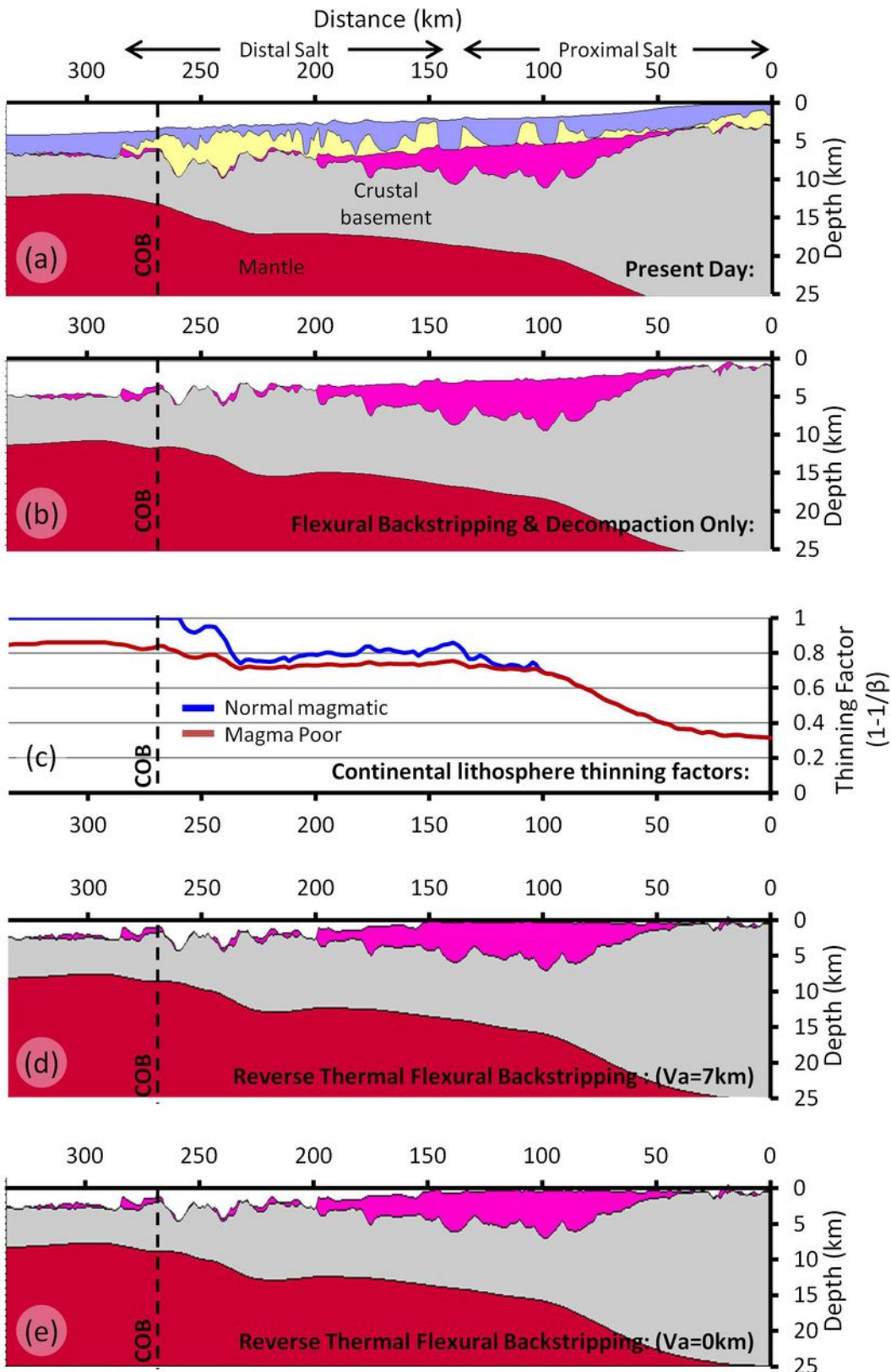


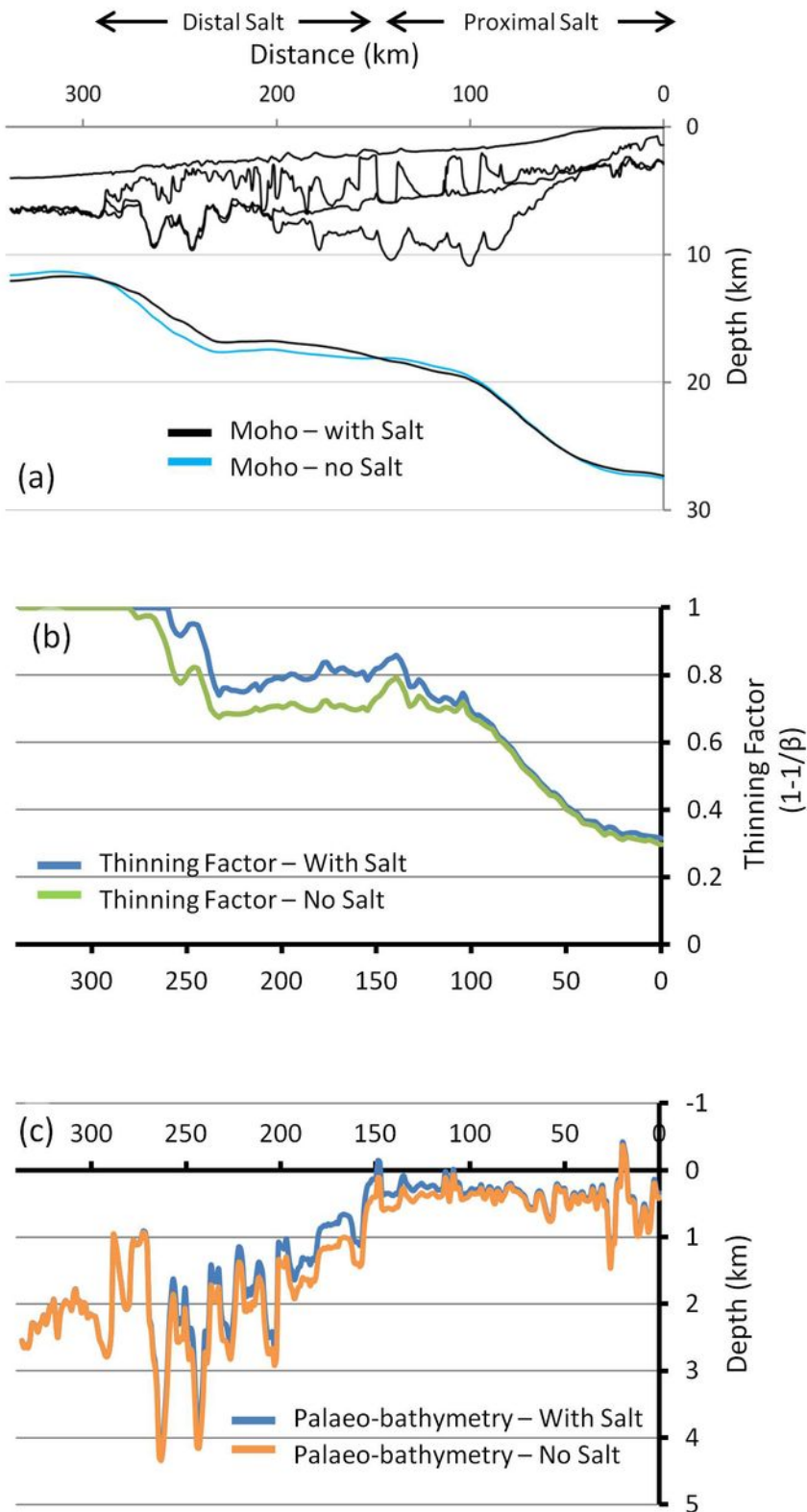




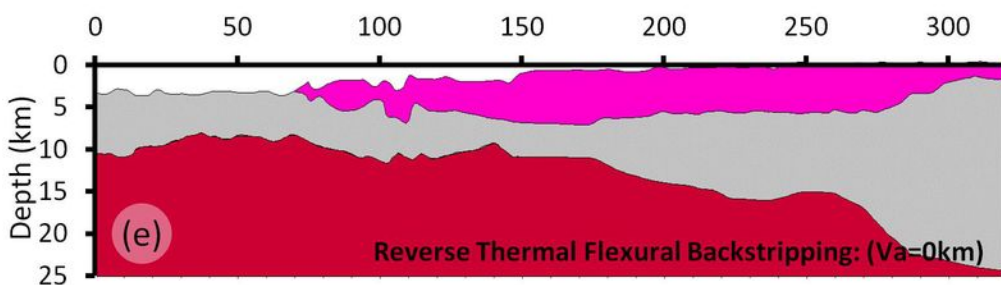
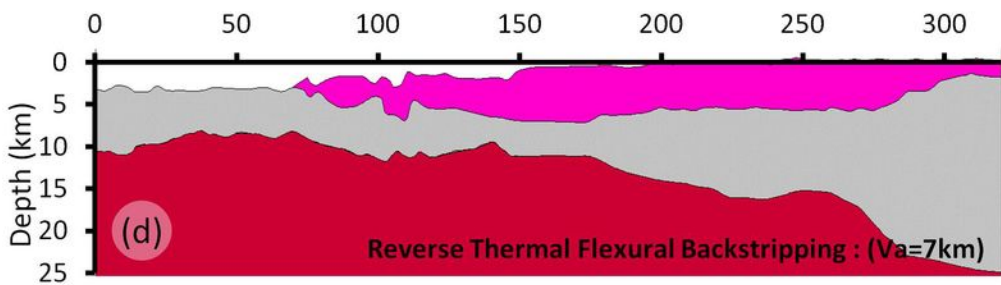
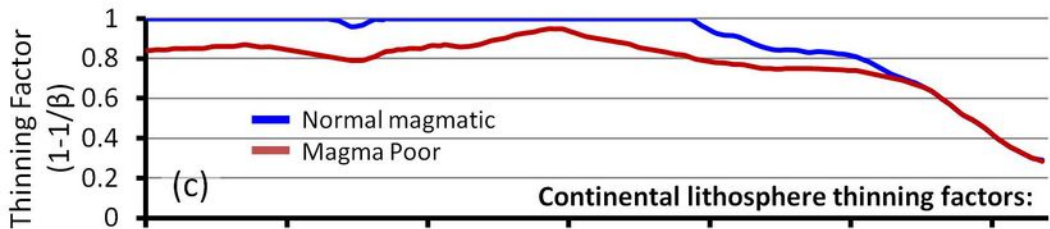
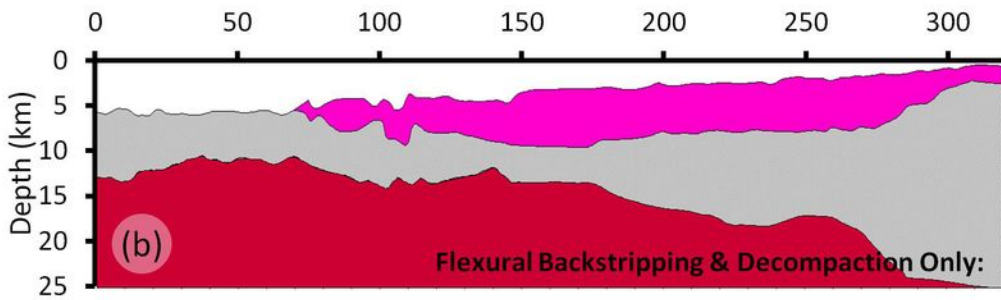
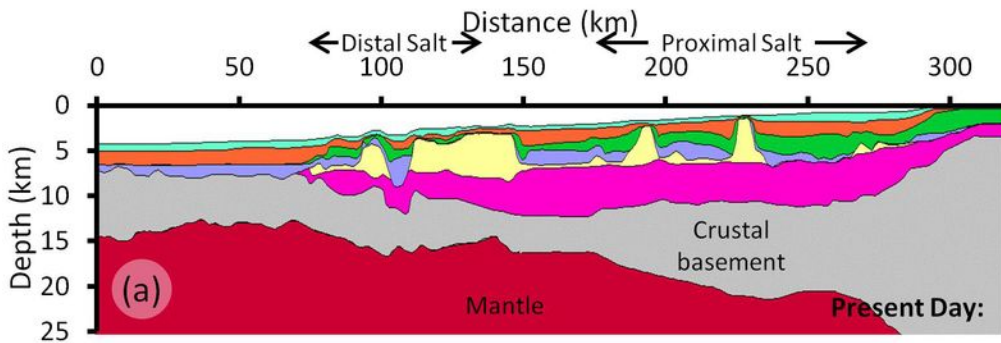


ION-GXT CS1-2400 profile:





P3 profile: (Moulin (2003) & Contrucci et al., (2004))





P7+11 profile (Moulin (2003) & Contrucci et al., (2004))

